Progress In Electromagnetics Research M, Vol. 80, 203–214, 2019

Analysis of Implantable Ultrasonic Coupling Wireless Power Transmission System

Xiaoheng Yan[1, 2], Zhengyin Zhu[1, 2, *], Guo-Qiang Liu[2, 3], and Xiaohe Zhao[2, 3]

Abstract—The research on implantable ultrasonic coupling wireless power transmission systems has not been systematically analyzed from the sound field theory, and the influencing factors of implanted ultrasonic coupling wireless power transmission systems based on the far-field model are proposed in this paper. Firstly, the far-field model is constructed. On this basis, the main factors affecting the ultrasonic energy transmission in the system are discussed. The COMSOL finite element simulation software was used to simulate the ultrasonic coupling wireless energy transmission system in human tissue environment, and the directivity of the energy transmission system was verified. The system experiment platform is built to analyze the energy transmission under different distances, different sound source frequencies, and different sound source excitations, and compare with the numerical simulation data. Finally, the influence of different factors on the energy transmission system is verified. It provides an effective reference for further research on implantable ultrasonic coupling wireless power transmission systems.

1. INTRODUCTION

With the development of technology and advances in medical care, implantable medical devices are playing an increasingly important role in the medical field. The power supply method of implantable medical equipment is relatively demanding, and the traditional wired energy supply method can no longer meet the needs of applications [1, 2]. The electromagnetic coupling wireless power transmission method developed in recent years has caused problems such as eddy current heating of skin and biological tissues [3–5]. The ultrasonic coupling wireless power transmission technology is a new type of non-contact power transmission method that uses ultrasonic waves as a carrier to convert electrical energy into acoustic energy through electro-acoustic conversion materials and convert acoustic energy into electrical energy through acoustic-electric conversion materials. Compared with the electromagnetic coupling wireless power transmission mode, the ultrasonic coupling wireless power transmission has the advantages of strong directivity, easy concentration of energy, sufficient distance of propagation, etc. [6, 7]. Besides, because ultrasonic coupling wireless power transmission uses ultrasonic waves for energy transmission, the transmission process does not generate electromagnetic radiation and eddy current heating effect. The ultrasonic coupling wireless power transmission can be applied to the metal environment or the demanding electromagnetic environment [8–10]. Therefore, the ultrasonic coupling wireless power transmission can make up for the shortage of the electromagnetic coupling wireless power transmission mode in the direction of power supply for implantable medical devices, and has broad application prospects [11–14].

Received 10 January 2019, Accepted 9 April 2019, Scheduled 26 April 2019

* Corresponding author: Zhengyin Zhu (ZhengyinZ@163.com).

[1] Faculty of Electrical and Control Engineering, Liaoning Technical University, Liaoning 125105, China. [2] Institute of Electrical Engineering, Chinese Academy of Science, Beijing 100190, China. [3] University of Chinese Academy of Sciences, Beijing 100049, China.

For the study of ultrasonic coupling wireless power transmission, Shmilovitz et al. used hysteresis control on the system circuit through the electromechanical equivalent model to adjust the system output power to achieve effective power at 85 mm implant depth [15]. Meng and Kiani used castor oil as the tissue model to optimize the transmission efficiency at a transmission distance of 3 cm to 6 cm by optimizing the implantation depth and load of the system [16]. Chou et al. used dual-port network analysis to achieve good transmission power and efficiency at a coupling distance of 9.5 mm to 15.5 mm by matching layer design of biological tissues [17]. Ozeri and Shmilovitz matched the acoustic impedance of the system by analyzing the acoustic link and obtained 70 mW of output power at a depth of 40 mm [20]. However, there is no relevant literature to systematically study the influencing factors of implantable ultrasonic coupling transmission system from the perspective of sound field. In view of this, this paper proposes an analysis of the ultrasonic coupling wireless power transmission system based on the sound field implanted in the biological tissue environment.

In this paper, the implanted ultrasonic coupling wireless power transmission system is studied. Firstly, the implanted ultrasonic far-field model is established. On this basis, the directivity of the sound field and the influence of distance, sound source frequency and sound source excitation on ultrasonic energy propagation are discussed. Finally, the influence of different influencing factors on the system is verified by COMSOL numerical simulation and experiment.

2. SOUND FIELD ANALYSIS OF IMPLANTABLE ULTRASONIC COUPLING WIRELESS POWER TRANSMISSION

2.1. Sound Field Model

The basic model of the implantable ultrasonic coupling wireless power transmission system is shown in Fig. 1. The transmitting transducer powered by the transmitting power module transmits ultrasonic waves, and the ultrasonic energy is transmitted to the receiving transducer in the human tissue. The receiving transducer converts the collected ultrasonic energy into electrical power. Finally, power is supplied to the human implantable device through the receiving power processing module. The transmitting power module generally uses a power amplifying circuit [9–11, 21–23] or an inverter circuit [7, 8, 13, 18–20] to supply power to the transmitting transducer, and the receiving power processing module mainly includes a rectifier circuit and a voltage-stabilizing circuit.

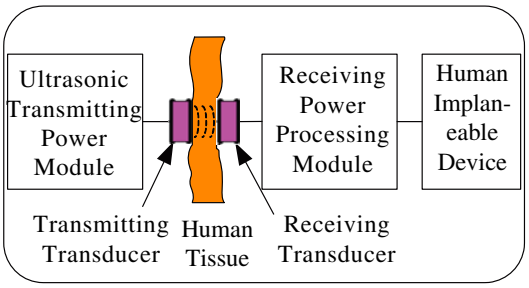

Figure 1. Model of the implantable ultrasonic coupling wireless power transmission system.

In this paper, the transmitting transducer is analogized to a circular planar piston sound source with a radius on the plane of infinite sound baffle. The maximum ultrasonic energy that can be received by the receiving transducer is the ultrasonic energy radiated by the transmitting transducer through the body tissue to the position of the receiving transducer. Ultrasonic energy is divided into two regions, far-field and near-field, according to the distance during the radiation process. As shown in Fig. 2, assume that the sound wave radiates along the z-axis, and the whole area is divided into near-field and far-field. The critical distance is,

$$z_g = \frac{a^2}{\lambda} \tag{1}$$

where a is the piston radius, and λ is the wavelength of the sound wave.

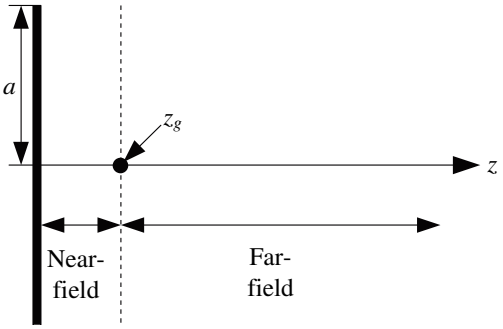

Figure 2. Far and near field of ultrasound radiation.

In the ultrasonic coupling wireless power transmission system, near-field characteristics are complex [25]. The transducer used has a radius about 2.5 cm, and the frequency is from 20 kHz to 40 kHz. The research distance is between 2 cm and 5 cm. In summary, the region of study is mostly in a far-field environment. Therefore, the study of the sound field in this paper is based on the far-field of sound and models the far-field of the piston.

2.2. Far-Field Characteristics of Sound

Figure 3 shows the sound field model of the ultrasonic coupling wireless transmitting and receiving transducers. Supposing that the sound source radius of the circular plane A is a, the center of the sound source is taken as the coordinate origin, and the plane A where the sound source is located is in the xoy plane. For the sound field of the parallel plane B whose distance from the plane A is d along the z-axis, and point Q is arbitrary point in plane B, the sound pressure of the A plane on the plane B at point Q can be obtained first. The sound intensity at point Q is also obtained, and then the sound intensity at point Q is integrated into the entire plane B. Thereby the sound energy of the sound field is obtained.

The distance from the origin to point Q is r, and the angle between the position vector $\mathbf{r}$ and z-axis is θ. When the sound source vibrates at velocity $u = u_a e^{j\omega t}$, the sound pressure at point Q is the integral of an infinite number of point sources on the piston surface. Assuming that the sound source

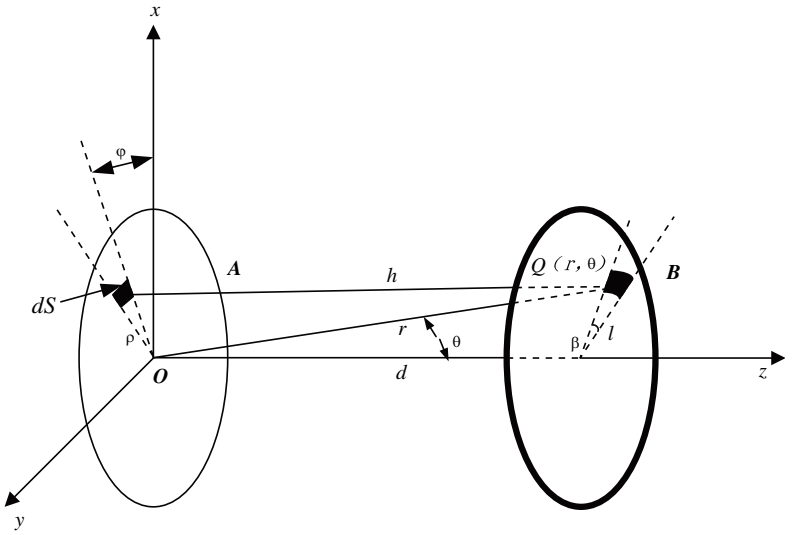

Figure 3. The sound field model of the ultrasonic coupling wireless transmitting and receiving transducers.

is the element dS with a radius of ρ from the center and an angle φ, and the point source strength is $dQ_0 = u_a dS$, the sound pressure at point Q is [24]

$$dx = j\frac{k\rho_0 c_0}{2\pi h} u_a dS e^{j(\omega t - kh)} \tag{2}$$

where h is the distance from element dS to point Q; $k = \frac{\omega}{c_0}$ is the wavenumber of sound field; u_a is the amplitude; ρ_0 is the density of the medium; c_0 is the sound velocity in the medium.

The total sound pressure of the entire sound source at point is [24]

$$p = \iint dp = \iint_S j\frac{k\rho_0 c_0}{2\pi h} u_a e^{j(\omega t - kh)} dS \tag{3}$$

Sound pressure is obtained after solving [24]

$$p = j\omega\frac{\rho_0 u_a a^2}{2r}\left[\frac{2J_1(ka\sin\theta)}{ka\sin\theta}\right] e^{j(\omega t - kr)} \tag{4}$$

where $J_1(ka\sin\theta)$ is the first order Bessel function.

Particle velocity is then found to be

$$v_r = -\frac{1}{j\omega\rho_0}\frac{\partial p}{\partial r} = \frac{1}{\rho_0 c_0}\left(1 + \frac{1}{jkr}\right) p \tag{5}$$

Sound intensity is

$$I_Q = \frac{1}{T}\int_0^T \mathrm{Re}\, p\, \mathrm{Re}\, v_r dt = \frac{1}{8}\rho_0 c_0 u_a^2 (ka)^2 \frac{a^2}{r^2}\left[\frac{2J_1(ka\sin\theta)}{ka\sin\theta}\right]^2 \tag{6}$$

where T is the signal period.

The point Q can be regarded as a sector on the plane B; the angle is β; the radius from the center of the circle is l; and the radiated sound power on the whole plane is

$$P = \iint_S IQdS = \int_0^{2\pi}\int_0^a \frac{1}{8}\rho_0 c_0 u_a^2 (ka)^2 \frac{a^2}{r^2}\left[\frac{2J_1(ka\sin\theta)}{ka\sin\theta}\right]^2 l dl d\beta \tag{7}$$

Simplification of Eq. (7)

$$P = \pi\rho_0 c_0 u_a^2 a^2 \int_0^a \frac{\left[J_1\left(ka\dfrac{l}{\sqrt{l^2+d^2}}\right]^2}{l} dl \tag{8}$$

with $r = \sqrt{l^2 + d^2}$, $\sin\theta = \frac{l}{\sqrt{l^2+d^2}}$.

Since the Bessel function is contained in Eq. (6), according to the Bessel function property, the sound intensity I has obvious directivity. The directivity is related to the relative ratio of the size of the sound source and wavelength (i.e., ka). As the value of ka increases, that is, as the size of the sound source increases or the radiation frequency increases, the directivity becomes stronger.

Meanwhile, it can be known from Eq. (8) that in an implantable ultrasonic coupling wireless power transmission system, given the transmission medium, the speed of sound, and the size of the transducer, the sound power received by receiving transducer is mainly affected by the transmission distance d, ultrasonic frequency ω, and excitation of the ultrasonic source.

3. SIMULATION AND EXPERIMENTAL VERIFICATION

3.1. Simulation Model Establishment and Verification

According to the environmental conditions of implantable ultrasonic coupling wireless power transmission system, model the system using COMSOL finite element simulation software. Different implantable devices have different depths from the outer skin. For example, an implantable Cardioverter-Defibrillator is implanted beneath the clavicle with the depth of around 10 mm; however, in the case

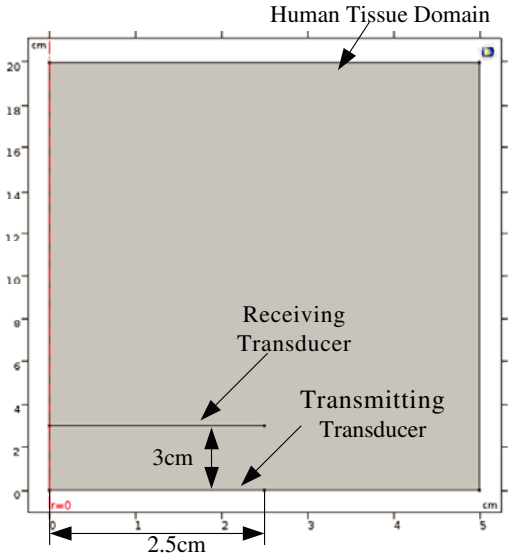

Figure 4. Simulation model of the implantable ultrasonic coupling wireless power transmission system.

of kidney, it is located about 50 mm depth from the outer skin [9]. So, the model is built according to actual needs, as shown in Fig. 4.

Using the 2-D axisymmetrical model in COMSOL, firstly, a $20\,cm \cdot 5\,\text{cm}$ human tissue domain is set up. A 2.5 cm radius ultrasonic transmitting transducer is placed near the symmetrical axis at the bottom of the region, using piezoelectric material PZT-5H, and a receiving transducer is placed 3 cm away from the transmitting transducer. The working principle of piezoelectric transducer is as follows [25].

$$\begin{cases} T_1 = c_{11}^E S_1 - e_{31} E_3 \\ D_3 = e_{31} S_1 + \varepsilon_{33}^E E_3 \end{cases} \tag{9}$$

where T_1 is the axial stress; S_1 is the stress-strain; c_{11}^E is the elastic stiffness (Young's modulus) of piezoelectric layer under constant electric field; e_{31} is the piezoelectric constants; E_3 is the electric field strength; D_3 is the electric displacement; ε_{33}^E is the dielectric constant under constant strain condition. Therefore, applying alternating voltage to piezoelectric material of piezoelectric transducer can cause displacement of piezoelectric material and then generate vibration velocity.

Secondly, because biological tissue can be treated as fluid under certain conditions [26], use the density of water medium, and according to the velocity of sound wave in human tissue, set the sound velocity to 1540 m/s as a simulation parameter [27]. The sound source at the transmitting end is set as a surface sound source, and the vibration velocity and frequency of the sound source can be adjusted within the required range.

In this paper, the directionality of the sound field is simulated and verified. When the excitation voltage is set to 50 V and the sound source frequency is 20 kHz, 28 kHz, and 40 kHz respectively, the simulation cloud images obtained by COMSOL are shown in Figs. 5(a), (b), and (c). At the same time, the sound intensity data drawing of each point on the receiving position at the corresponding frequency is extracted as shown in Fig. 5(d).

As can be seen in Fig. 5(d), the sound intensity at the receiving end gradually decreases with increasing distance from the symmetry axis (i.e., the center position), which indicates that the sound field has directivity in the process of propagation. At the same time, as the ultrasonic frequency increases, the faster the sound intensity decays, the more obvious the change is, which is also consistent with Eq. (6) where the larger the frequency is, the greater the directivity is.

From the sound intensity clouds in Figs. 5(a), (b), and (c) at three different frequencies, it can be seen that when the transmitting end frequency is 20 kHz, the sound intensity concentrated region has a short distance along the propagation direction and is dispersed to the periphery. From 20 kHz

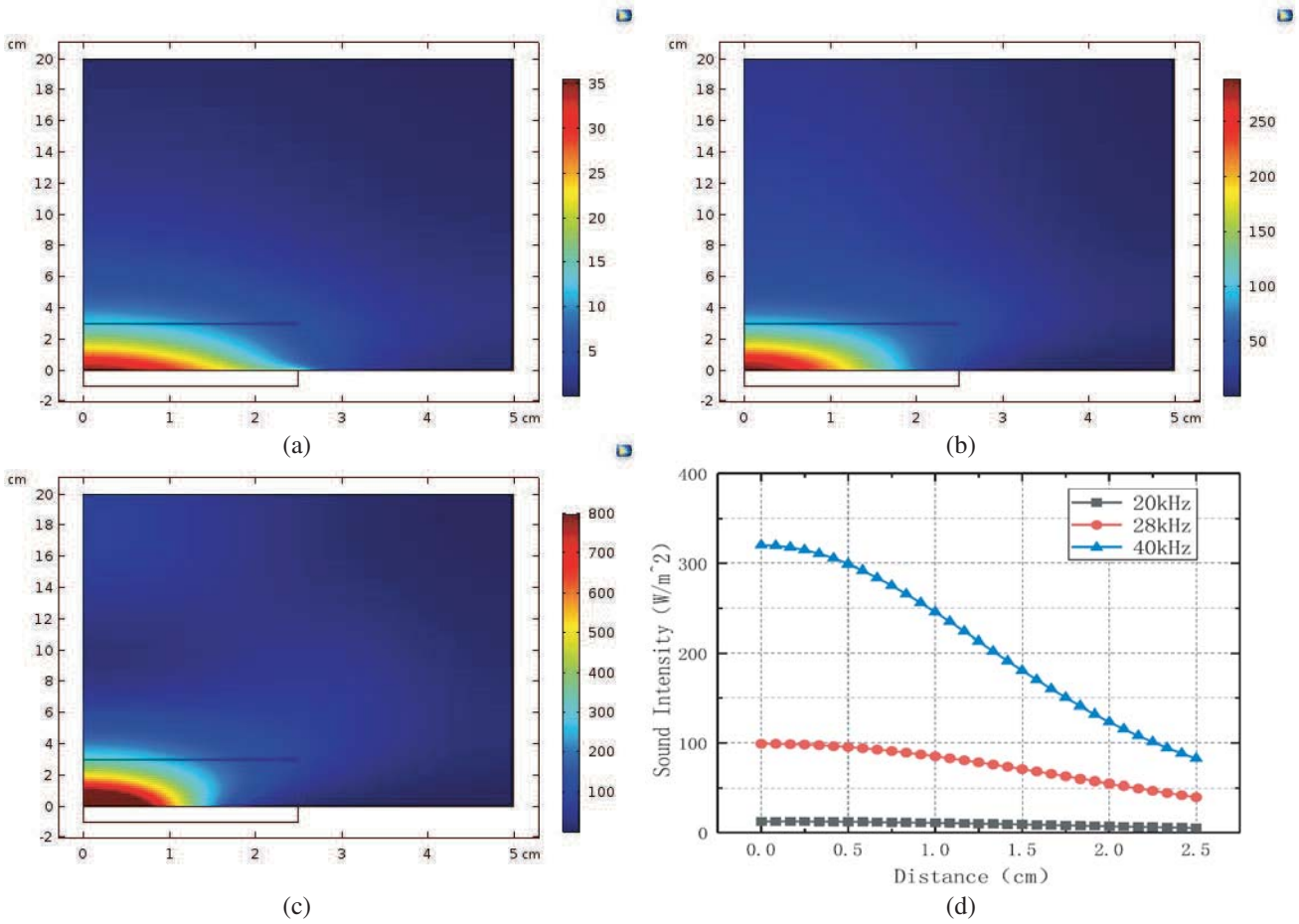

Figure 5. Simulation sound intensity with the source frequency (a) 20 kHz, (b) 28 kHz and (c) 40 kHz, (d) sound intensity data curves at receiving points at different frequencies.

to 28 kHz to 40 kHz, the concentrated area of sound intensity gradually extends along the direction of sound wave propagation, and the lateral direction gradually becomes narrow. This also shows that the directionality of the sound field is stronger as the frequency increases.

3.2. Experimental Verification

In order to verify the influence of ultrasonic energy with distance, ultrasonic frequency and excitation intensity of ultrasonic source on system energy transmission in implantable ultrasonic coupling wireless power transmission system, an ultrasonic energy transmission system by pork tissue was constructed, as shown in Fig. 6. Limited by the conditions of ultrasonic transducer and power amplifier, the parameters of this experimental platform are shown in Table 1.

(1) Influence of distance on ultrasonic energy propagation

Experiments were carried out using a 20 kHz, 28 kHz, 40 kHz transducer for ultrasonic energy transfer experiments of different thicknesses of pork tissue. The excitation voltage at the transmitting end was 50 V, and the transducer at the receiving end was connected to a 50 Ω resistive load. By detecting the voltage value at the load end, it can be transformed into the power of the load. In the COMSOL simulation model, ultrasonic waves with a frequency of 20 kHz, 28 kHz, 40 kHz and an excitation voltage of 50 V are applied at the transmitting end, and change data of the sound intensity at the different distances of the transducer at the receiving end are collected.

In order to facilitate data comparison, the simulated and experimental data are normalized, and

Table 1. Parameters of experimental platform.

parameters	value
Transmitting frequency	20 kHz; 28 kHz; 40 kHz
Transmitting voltage (peak-to-peak voltage value)	30 V to 50 V
Thicknesses of pork tissue	1.5 cm to 5 cm
Transducer radius	2.5 cm
load	50 Ω

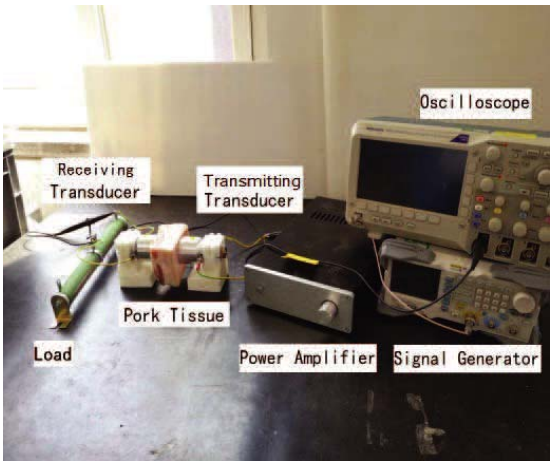

Figure 6. Experimental platform of implantable ultrasonic coupling wireless power transmission system.

the normalization formula is

$$x^* = \frac{x - x_{\min}}{x_{\max} - x_{\min}} \tag{10}$$

where x^* is the normalized value, x the value to be normalized, $x_{\min}$ the minimum value in the data to be normalized, and $x_{\max}$ the maximum value in the data to be normalized.

The data before and after normalization are shown in Table 2 below.

The influence of the distance on the ultrasonic energy is shown in Fig. 7. In Fig. 7, the horizontal axis represents the distance from the receiving transducer to the transducer of the transmitting end, and the vertical axis represents the power after normalization. It can be seen from Table 2 and Fig. 7 that when the frequency is 20 kHz and the distance 1.8 cm, the maximum transmission power is 1.60 W. As the distance increases, the power received by the receiving end gradually decreases. At different frequencies, when the frequency is 28 kHz, the maximum power of 1.92 W is obtained at 1.8 cm, and at 40 kHz, the maximum power of 3.31 W is obtained at 1.8 cm. At the same time, it can be seen that the simulation and experiment are consistent from the normalized simulation data and experimental data trends in Fig. 7.

(2) Influence of sound source frequency on ultrasonic energy propagation

In order to verify the influence of different frequencies on the ultrasonic transmission power, the transducers with frequencies of 20 kHz, 25 kHz, 28 kHz, 33 kHz, and 40 kHz were used in the experiment. The excitation voltage was 50 V, and the ultrasonic energy of pork tissue with a thickness of 3 cm from the transmitter was collected. The simulation data are the sound intensity data at the transmitting transducer excitation voltage of 50 V, the sound source frequencies of 20 kHz, 25 kHz, 28 kHz, 33 kHz, and 40 kHz, and the transducer position of 3 cm from the transmitting end. The two data are also normalized, and the data in Table 3 below are obtained.

Table 2. Normalized data of sound field energy at different distances.

a. 20 kHz Normalized Power Data

Distance (cm)	Prenormalized simulation data (W)	Normalized simulation data	Prenormalized experimental data (W)	Normalized experimental data
1.8	12.07	1	1.60	1
2.2	10.57	0.79	1.38	0.84
2.6	9.29	0.61	1.16	0.67
3	8.22	0.46	0.96	0.52
3.4	7.34	0.33	0.81	0.40
3.8	6.60	0.23	0.66	0.29
4.2	5.98	0.14	0.52	0.19
4.6	5.45	0.06	0.40	0.09
5	5.0	0	0.27	0

b. 28 kHz Normalized Power Data

Distance (cm)	Prenormalized simulation data (W)	Normalized simulation data	Prenormalized experimental data (W)	Normalized experimental data
1.8	28.08	1	1.92	1
2.2	24.53	0.79	1.62	0.81
2.6	21.45	0.61	1.38	0.65
3	18.83	0.46	1.16	0.51
3.4	16.64	0.33	1.00	0.40
3.8	14.80	0.22	0.83	0.29
4.2	13.27	0.13	0.67	0.19
4.6	12.01	0.06	0.52	0.10
5	10.97	0	0.37	0

c. 40 kHz Normalized Power Data

Distance (cm)	Prenormalized simulation data (W)	Normalized simulation data	Prenormalized experimental data (W)	Normalized experimental data
1.8	78.44	1	3.31	1
2.2	68.61	0.81	3.04	0.90
2.6	60.06	0.64	2.49	0.70
3	52.65	0.49	2.03	0.54
3.4	46.22	0.37	1.72	0.43
3.8	40.62	0.25	1.42	0.32
4.2	35.74	0.16	1.12	0.21
4.6	31.46	0.07	0.83	0.10
5	27.68	0	0.54	0

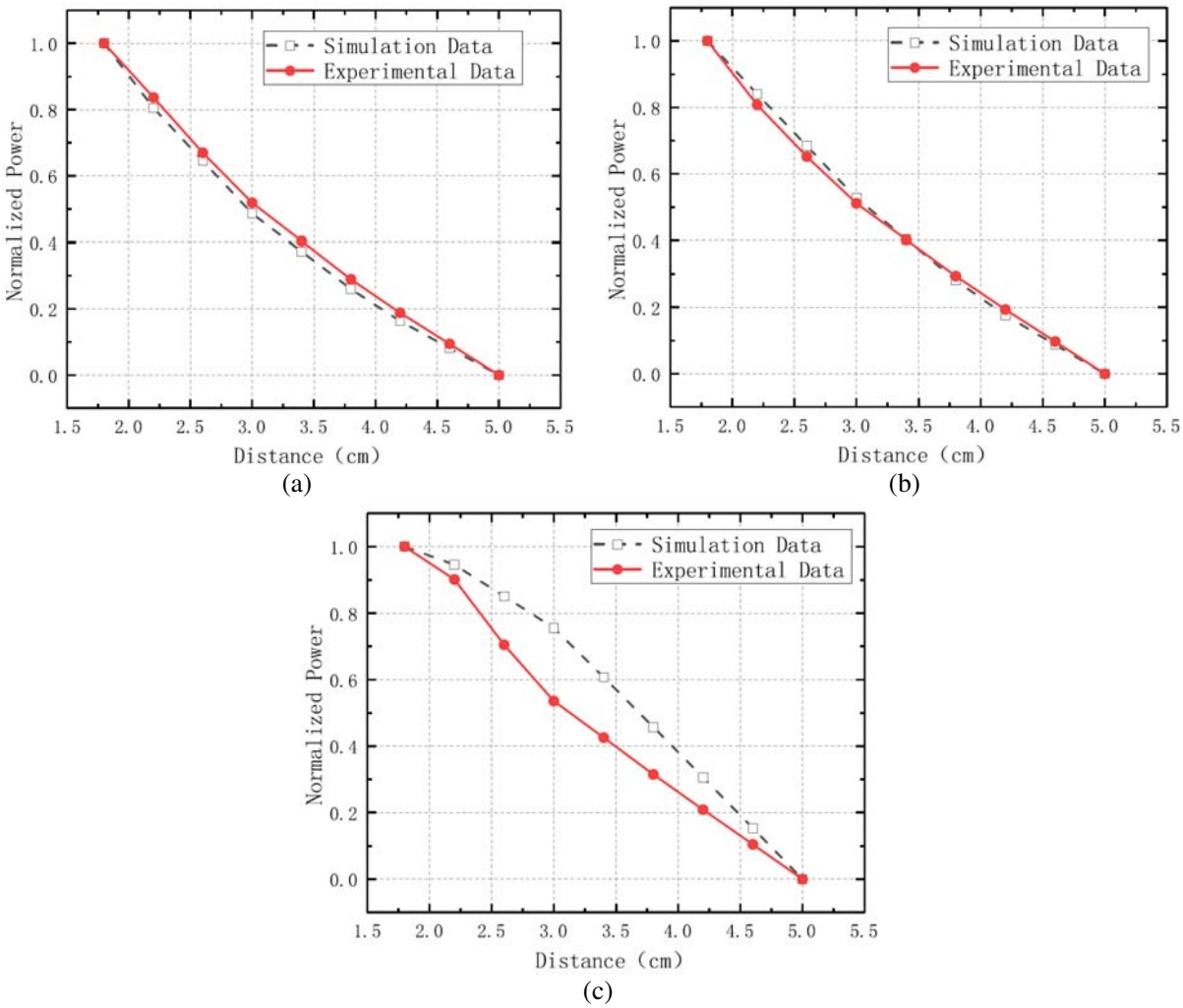

Figure 7. Curves of ultrasound energy with distance at (a) 20 kHz, (b) 28 kHz and (c) 40 kHz.

Table 3. Normalized power data of sound field energy at different frequencies.

Frequency (kHz)	Prenormalized simulation data (W)	Normalized simulation data	Prenormalized experimental data (W)	Normalized experimental data
20	8.22	0	1.01	0
25	13.00	0.11	1.31	0.27
28	18.83	0.24	1.34	0.30
33	33.00	0.56	1.67	0.60
40	52.65	1	2.12	1

Using the normalized data in Table 3, the relationship between ultrasonic energy and frequency in experiment and simulations at different frequencies can be obtained. As shown in Fig. 8, the horizontal axis represents the ultrasonic emission frequency of the transmitting transducer, and the vertical axis is the normalized ultrasonic power. From the data in Table 3 and Fig. 8, it can be seen that within the experimental range, the received power is the largest at 3 cm from transmitting end, and the maximum

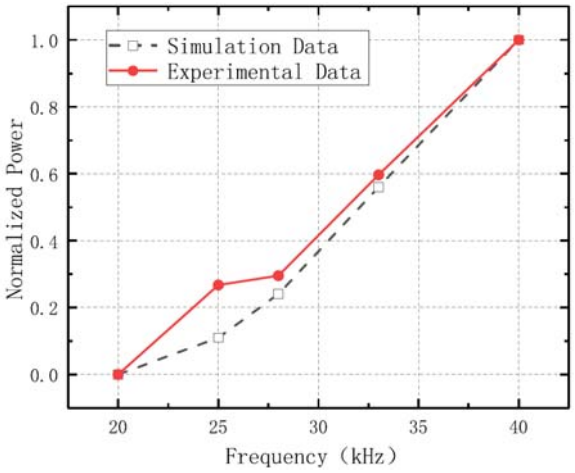

Figure 8. Curves of ultrasound energy with frequency at a distance of 3 cm.

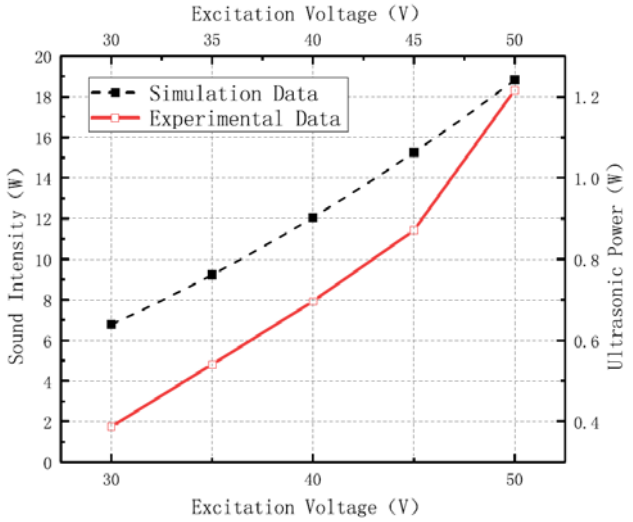

Figure 9. Curves of ultrasound energy with excitation source amplitude.

received power is 2.12 W. At 20 kHz, the received power is at a minimum of 1.01 W. Influenced by factors such as transducer performance and distance change caused by softness of pork tissue, the curve of the normalized power of the experimental data varying with frequency deviates from the simulation results, but the overall trend is still increasing. Therefore, in the test frequency range, at the same position, as the frequency increases, the ultrasonic energy received by the receiving end also gradually increases.

(3) The effect of the excitation source size on energy propagation

Figure 9 is a comparison curve of experimental and simulated data of ultrasonic energy under different excitation source amplitudes. The experimental data are the ultrasonic power measured at the receiving end at different excitation voltages when the transmitting transducer frequency is 28 kHz through 3 cm of pork tissue. The simulation data are the sound intensity of the transmitting transducer when the source frequency of the transducer is 28 kHz, and the vibration velocity is changed from 30 V to 50 V. In Fig. 9, the horizontal axis of the bottom end is the excitation level applied by the COMSOL simulation transmitting end; the left vertical axis represents the sound intensity of the COMSOL simulation part; the top horizontal axis is the excitation voltage of the transmitting transducer in the experiment; and the right vertical axis represents the ultrasonic power obtained by the receiving transducer in the experiment. Fig. 9 shows that experimental and simulated data are consistent with trends in sound source size. In the far field, the energy tends to increase with the increase of the excitation source at the transmitting end.

4. CONCLUSION

In this paper, an implantable ultrasonic coupling wireless power transmission system is approximated as a far field model of sound for mathematical research. The simulation is carried out by using COMSOL, and compared with the experiment, the following conclusions are drawn: (1) the implantable ultrasonic coupling wireless power transmission system sound field has a directivity. (2) The sound field energy is affected by factors such as distance, sound source frequency, and sound source excitations. In the research range, the ultrasonic energy received by the receiving transducer exhibits a decreasing trend with increasing distance. At the same time, with the increase of source frequency and source size, it shows an increasing trend. These conclusions provide a theoretical basis for the study of implantable ultrasonic coupling wireless power transmission system from the direction of the sound field and promote the further development of power supply methods for implantable devices based on ultrasonic power transmission.

REFERENCES

1. Xiong, H., S. Meng, L. Liu, et al., "Design of wireless power transfer for implantable medical devices inweak power receiving," *Journal of Tianjin Polytechnic University*, Vol. 36, No. 03, 60–64, 2017.
2. Zhang, B., X. Shu, and R. Huang, "The development of inductive and resonant wireless power transfer technology," *Transactions of China Electrotechnical Society*, Vol. 32, No. 18, 3–17, 2017.
3. Cheng, S., X. Chen, J. Wang, et al., "Key technologies and applications of wireless power transmission," *Transactions of China Electrotechnical Society*, Vol. 30, No. 19, 68–84, 2015.
4. Li, Q., S. Chen, W. Wang, et al., "Parameter optimization of magnetic coupling energy transfer for active implantable systems," *Journal of Tsinghua University (Natural Science Edition)*, Vol. 55, No. 03, 351–355, 2015.
5. Yin, C. and B. Xu, "Wireless power transfer for implantable ventricular assistance: A review," *Transactions of China Electrotechnical Society*, Vol. 30, No. 19, 103–109, 2015.
6. Roes, M. G. L., M. A. M. Hendrix, and J. L. Duarte, "Contactless energy transfer through air by means of ultrasound," *IECON 2011 — 37th Annual Conference of the IEEE Industrial Electronics Society*, 1238–1243, Melbourne, VIC, 2011.
7. Zhang, J., X. Huang, Y. Zou, et al., "Feasibility of ultrasonic wireless power transmission," *Advanced Technology of Electrical Engineering and Energy*, Vol. 30, No. 02, 66–69+74, 2011.
8. Dai, X., L. Li, Y. Li, et al., "Determining the maximum power transfer condition for ultrasonic power transfer system," *2016 IEEE 2nd Annual Southern Power Electronics Conference (SPEC)*, 1–6, Auckland, 2016.
9. Lee, S. Q., W. Youm, and G. Hwang, "Biocompatible wireless power transferring based on ultrasonic resonance devices," *ICA 2013 Montreal Montreal*, 2–7, Canada, Jun. 2013.
10. Ishiyama, T., Y. Kanai, J. Ohwaki, and M. Mino, "Impact of a wireless power transmission system using an ultrasonic air transducer for low-power mobile applications," *IEEE Symposium on Ultrasonics*, 1368–1371, Vol. 2, 2003.
11. Awal, Md. R., M. Jusoh, T. Sabapathy, M. R. Amarudin, and R. A. Rahim, "State-of-the-art develop-ments of acoustic energy transfer," *International Journal of Antennas and Propagation Volume 2016*, Article ID 3072528, 14 pages, 2016.
12. Kim, C., et al., "Design of miniaturized wireless power receivers for mm-sized implants," *2017 IEEE Custom Integrated Circuits Conference (CICC)*, 1–8, Austin, TX, 2017.
13. Shahab, S., M. D. Gray, and Erturk, "Ultrasonic power transfer from a spherical acoustic wave source to a free-free piezoelectricreceiver: Modeling and experiment," *Journal of Applied Physis*, Vol. 117, No. 10, 2015.
14. Hori, Y., Y. Shigeta, K. Fujimori, et al., "Design of anti-resonance transducer and its abilities for efficient ultrasonic wireless power transmission system," *2011 41st European Microwave Conference*, 67–70, Manchester, 2011.
15. Shmilovitz, D., S. Ozeri, C.-C. Wang, and B. Spivak, "Noninvasive control of the power transferred to an implanted device by an ultrasonic transcutaneous energy transfer link," *IEEE Transactions on Biomedical Engineering*, Vol. 61, No. 4, 995–1004, Apr. 2014.
16. Meng, M. and M. Kiani, "A hybrid inductive ultrasonic link for wireless power transmission to millimeter-sized biomedical implants," *IEEE Transactions on Circuits and Systems II: Express Briefs*, Vol. 64, No. 10, 1137–1141, Oct. 2017.
17. Chou, T.-C., R. Subramanian, J. Park, and P. P. Mercier, "A miniaturized ultrasonic power delivery system," *2014 IEEE Biomedical Circuits and Systems Conference (BioCAS) Proceedings*, 440–443, Lausanne, 2014.
18. Fai, L. H., D. Xin, and H. Aiguo, "Electrical modeling of a wireless ultrasonic power transfer system," *Transactions of China Electrotechnical Society*, Vol. 30, No. 19, 85–89, 2015.
19. Leung, H. F. and A. P. Hu, "Modeling the contact interface of ultrasonic power transfer system based on mechanical and electrical equivalence," *IEEE Journal of Emerging and Selected Topics in Power Electronics*, Vol. 6, No. 2, 800–811, Jun. 2018.

20. Ozeri, S. and D. Shmilovitz, "Ultrasonic transcutaneous energy transfer for powering implanted devices," *Ultrasonics*, Vol. 50, No. 6, 556–566, 2014.
21. Mehdizadeh, E. and G. Piazza, "Chip-scale near-field resonant power transfer via elastic waves," *Journal of Microelectromechanical Systems*, Vol. 26, No. 5, 1155–1164, Oct. 2017.
22. Guida, R., G. E. Santagati, and T. Melodia, "A 700 kHz ultrasonic link for wireless powering of implantable medical devices," *2016 IEEE Sensors*, 1–3, Orlando, FL, 2016.
23. Maleki, T., N. Cao, S. H. Song, et al., "An ultrasonically powered implantable micro-oxygen generator (IMOG)," *IEEE Transactions on Biomedical Engineering*, Vol. 58, No. 11, 3104–3111, Nov. 2011.
24. Du, G., Z. Zhu, and X. Gong, *Acoustic Basis*, 212–235, Nanjing University Press, Nanjing, 2012.
25. Xu, Q., L. Ge, C. Zong, et al., "Design of self-powered power supply of sensor for piezoelectric energy," *Piezoelectrics & Acoustooptics*, 1–4, 2019.
26. Liu, G. Q., *Magnetoacoustic Tomography Technology*, 142–156, Science Press, Beijing, 2014.
27. Chen, A., X. Chen, and C. Dong, "Application value of sound velocity matching technology in imaging normal human tissues and organs," *Journal of Practical Medicine*, Vol. 30, No. 19, 3139–3141, 2014.